^{18}F-Tetrafluoroborate, a PET Probe for Imaging Sodium/Iodide Symporter Expression: Whole-Body Biodistribution, Safety, and Radiation Dosimetry in Thyroid Cancer Patients

Jim O'Doherty[1], Maite Jauregui-Osoro[1], Teresa Brothwood[2], Teresa Szyszko[1], Paul K. Marsden[1], Michael J. O'Doherty[1], Gary J.R. Cook[1], Philip J. Blower[1], and Val Lewington[2]

[1]PET Imaging Centre, Division of Imaging Sciences and Biomedical Engineering, King's College London, St. Thomas' Hospital, London, United Kingdom; and [2]Department of Nuclear Medicine, Guy's & St. Thomas' Hospital NHS Foundation Trust, Great Maze Pond, London, United Kingdom

We report the safety, biodistribution, and internal radiation dosimetry, in humans with thyroid cancer, of ^{18}F-tetrafluoroborate (^{18}F-TFB), a novel PET radioligand for imaging the human sodium/iodide symporter (hNIS). **Methods:** Serial whole-body PET scans of 5 subjects with recently diagnosed thyroid cancer were acquired before surgery for up to 4 h after injection of 184 ± 15 MBq of ^{18}F-TFB. Activity was determined in whole blood, plasma, and urine. Mean organ-absorbed doses and effective doses were calculated via quantitative image analysis and using OLINDA/EXM software. **Results:** Images showed a high uptake of ^{18}F-TFB in known areas of high hNIS expression (thyroid, salivary glands, and stomach). Excretion was predominantly renal. No adverse effects in relation to safety of the radiopharmaceutical were observed. The effective dose was 0.0326 ± 0.0018 mSv/MBq. The critical tissues/organs receiving the highest mean sex-averaged absorbed doses were the thyroid (0.135 ± 0.079 mSv/MBq), stomach (0.069 ± 0.022 mSv/MBq), and salivary glands (parotids, 0.031 ± 0.011 mSv/MBq; submandibular, 0.061 ± 0.031 mSv/MBq). Other organs of interest were the bladder (0.102 ± 0.046 mSv/MBq) and kidneys (0.029 ± 0.009 mSv/MBq). **Conclusion:** Imaging using ^{18}F-TFB imparts a radiation exposure similar in magnitude to many other ^{18}F-labeled radiotracers. ^{18}F-TFB shows a biodistribution similar to ^{99m}Tc-pertechnetate, a known nonorganified hNIS tracer, and is pharmacologically and radiobiologically safe in humans. Phase 2 trials for ^{18}F-TFB as an hNIS imaging agent are warranted.

Key Words: ^{18}F-TFB; thyroid imaging; PET/CT

J Nucl Med 2017; 58:1666–1671
DOI: 10.2967/jnumed.117.192252

The human sodium/iodide symporter (Na^+/I^-; hNIS) is a plasma membrane glycoprotein that mediates active I^- transport into thyroid epithelial and follicular cells. It also mediates transport of I^- into cells of other tissues that do not organify iodide, such as the salivary glands, gastric mucosa, and breast (*1*). As a target for molecular imaging, its main clinical role has been in investigation of thyroid pathophysiology. Radioiodine has historically been used for both diagnostic thyroid imaging (using ^{123}I-I^-) and treatment of benign and malignant thyroid disease (using ^{131}I-I^-) (*2*). Because of its similarity of volume and charge with iodide ions, ^{99m}Tc-$NaTcO_4^-$ (sodium pertechnetate) is also widely used to study thyroid function. To overcome the limitations of γ-camera planar and single photon emission tomography imaging with respect to resolution and sensitivity, recent interest has focused on developing PET tracers for thyroid imaging.

Phan et al. reported that ^{124}I-I^- PET was a more sensitive diagnostic tool than ^{131}I-I^- scintigraphy in 20 patients (*3*). A study by Gulec et al. with ^{124}I-I^- PET identified 22.5% more iodine-avid foci than with planar ^{131}I-I^- scintigraphy after treatment (*4*). However, the complex decay scheme of ^{124}I (*5*) and low positron abundance result in poor PET imaging characteristics. Optimal target-to-background ratios are reported after 24 h. ^{124}I requires a complex cyclotron-based production and purification process (*6*) and because of its relatively long half-life of 4.2 d leads to a high effective dose (0.095–1.5 mSv/MBq) (*7*). Because of the superior PET imaging characteristics and dosimetry of ^{18}F, a reliable and sensitive ^{18}F-based radioligand for hNIS would have potential for molecular imaging of hNIS activity. Several small anionic species containing fluorine, such as tetrafluoroborate (BF_4^-), fluorosulfate (SO_3F^-), hexafluorophosphate (PF_6^-), and difluorophosphate ($PO_2F_2^-$) have been identified as hNIS substrates (*8,9*). Although ^{18}F-SO_3F^- was only recently synthesized for the first time and shown to be an effective high-affinity NIS tracer in mice (*10*), the earliest reports of ^{18}F-BF_4^- date from the 1960s (*11–13*). Our group recently developed a method for the synthesis of ^{18}F-tetrafluoroborate (^{18}F-TFB) suitable for routine clinical production and showed it to be a tracer for hNIS, with a biologic behavior similar to ^{99m}Tc-TcO_4^- in vitro and in mice (*14–16*). Marti-Climent et al. detailed the characteristic biodistribution of ^{18}F-TFB in NIS-expressing tissues in cynomolgus primates, with uptake in the thyroid, stomach, and salivary glands, and a mean whole-body absorbed dose of 0.0247 mSv/MBq (*17*). Given the potential of an ^{18}F-based radioligand for diagnosis and treatment planning in thyroid disease, we investigated the safety, biodistribution, and radiation dosimetry of ^{18}F-TFB in a human population.

MATERIALS AND METHODS

Radiopharmaceutical Preparation

Synthesis of the ^{18}F-TFB IMP (Investigational Medicinal Product) was performed by a method similar to a previously described automated labeling protocol (*14*) using an Eckert and Ziegler Modular-Lab synthesis unit (Imaging Equipment Ltd.). ^{18}F-fluoride (46 ± 6 GBq),

Received Feb. 23, 2017; revision accepted Apr. 1, 2017.
For correspondence or reprints contact: Val Lewington, Department of Nuclear Medicine, Guy's Hospital, Great Maze Pond, London, U.K.
E-mail: val.lewington@gstt.nhs.uk
Published online Apr. 6, 2017.

obtained from proton-irradiated ^{18}O-water (98 atom% [Rotem Industries Ltd.]; 11-MeV protons from a CTI RDS 112 cyclotron; beam current, 30 μA; irradiation time, 60 min), was trapped in a QMA cartridge (Sep-Pak Light QMA cartridge; Waters) conditioned with 1.0 M sodium hydrogen carbonate (10 mL, Ph Eur; Merck) followed by water for injections (10 mL, BP, Hamelin Pharmaceuticals) and air (10 mL). Hydrochloric acid (1.5 M, 1.2 mL), prepared by dilution of hydrochloric acid fuming 37% (Ph Eur; Merck) with water for injections (BP, Hamelin Pharmaceuticals), was then passed through the QMA cartridge, eluting the ^{18}F-fluoride into the reactor, which contained sodium tetrafluoroborate (Sigma-Aldrich) (1 mg in 0.1 mL water for injections). The reaction mixture (1.3 mL) was heated to 80°C for 15 min, cooled to 20°C, and passed through a silver ion-loaded cation exchange cartridge (OnGuard II AG [Dionex], conditioned with 10 mL of water and 5 mL of air) to remove chloride ions and raise the pH, and through 2 alumina cartridges (SepPak Light Alumina N [Waters], conditioned with 10 mL of water and 5 mL of air) to remove unreacted ^{18}F-fluoride. The product was eluted with water for injections (2 mL) into a nitrogen-filled USP type 1 glass sterile vial (N46; GE Healthcare) containing water for injections (2 mL). After production, the vial containing the unfiltered product (5.3 mL) was transferred to a sterile isolator, for sterile filtration and quality control sampling. The process was validated to demonstrate that ^{18}F-TFB can be consistently manufactured on the Modular-Lab synthesizer to meet the required quality control release specifications. Stability studies were conducted by testing an aliquot from the validation batches for radiochemical purity and pH at 2, 4, and 6 h from the end of synthesis.

Radiopharmaceutical Quality Control

Radiochemical identity, purity, and specific activity of the final product were checked by ion chromatography (930 Compact IC Flex; Metrohm) with in-line conductimetric and γ-detectors (B-FC-3200; LabLogic) using a Shodex IC I-524A column (4.6 × 100 mm) with 2.5 mM phthalic acid (adjusted to pH 4.0 with tris[hydroxymethyl] aminomethane) as eluent. The flow rate was 1.5 mL/min, and column temperature was 40°C. The ion chromatography quality control method was validated following the International Conference on Harmonisation guidelines, and the concentration of $^{19/18}$F-BF_4- in the final product was determined from the ion chromatogram by reference to a calibration curve. Radio–thin-layer chromatography (TLC) was performed using a silica gel stationary phase (Silica gel 60 F_{254}, 5 × 10 cm; Merck) with methanol as the mobile phase. Plates were scanned using a radio-TLC scanner (Scan-RAM; LabLogic) with a β^+ probe (PS Plastic-PM; LabLogic). The radiochemical purity of the product was determined as the radioactivity associated with the tetrafluoroborate peak ($Rf = 0.6$, c.f. $Rf = 0$ for fluoride) as a percentage of the total chromatogram radioactivity. Silver content was determined using Quantofix Silver test strips (Macherey-Nagel). The bacterial endotoxin assay was performed using the Endosafe Portable Test System (Charles River) using limulus amebocyte lysate reagent water and licensed Endosafe Portable Test System cartridges (Charles River) with a sensitivity of 0.05–5.0 EU/mL. The integrity of the sterilizing filters was tested after use with the bubble point method, and sterility testing was performed by Wickham Laboratories.

Patients

Patients were recruited in accordance with the European Council Directive. The clinical protocol was approved by the local Research Ethics Committee (reference no. 14/LO/1247, ISRCTN: 75827286). All patients provided written informed consent.

Five subjects (2 men, 3 women; average age, 46 y) with newly diagnosed, cytologically confirmed thyroid cancer were imaged before elective total thyroidectomy and ^{131}I-NaI thyroid remnant ablation. Pregnant and lactating women were excluded.

A cannula was placed in a vein in the antecubital fossa of each arm, one for injection of ^{18}F-TFB and the other for withdrawal of venous blood. Electrocardiographic monitoring, pulse, blood pressure, body temperature (using a temperature strip on the patient's forehead), and respiratory rate were monitored throughout the study.

PET/CT Data Acquisition

Bolus injection of ^{18}F-TFB (mean ± SD, 185 ± 15 MBq) was performed with the patient positioned on the scanning couch. Imaging comprised a 90-min series of 7 sequential whole-body PET/CT scans (from head to foot), followed by 2 further whole-body PET/CT scans at 120 and 240 min after injection (Fig. 1) with a Discovery 710 PET/CT scanner (GE Healthcare) with an axial field of view of 15.7 cm. Each scan covered the vertex to midthigh, with an 11-slice overlap between bed positions. Three low-dose whole-body CT scans (140 kV, 10 mA, 0.5-s rotation time, 40-mm collimation) were obtained, one before the block of 7 sequential scans and then one before each of the scans at 120 and 240 min, for attenuation correction and anatomic reference. The initial 1 min per bed scan duration was adjusted to compensate for radioactive decay up to a maximum of 3 min per bed step for the final scan at 240 min.

Quantification of Blood and Urine Data

Venous blood samples (5 mL each) were acquired at 0, 1, 2, 5, 10, 20, 40, 60, 90, 120, and 240 min after injection. Three 0.2-mL aliquots from each blood sample were weighed and counted on a 10-sample well counter (2470 WIZARD2; PerkinElmer), previously cross-calibrated with ^{18}F to the PET scanner using a standard calibration technique subject to daily quality control. Whole-blood samples were centrifuged for 5 min (6,000 rpm), and three 0.2-mL samples of plasma from each were then counted in the well-counter. Following the method of Namias et al. (*18*), the distribution ratio, *R(t),* between blood cells and plasma can be calculated from experimental measurements of the whole-blood and plasma activity concentrations (C_{WB} and C_P, respectively) at each time point using the equation:

$$R(t) = C_{BC}(t)/C_P(t), \qquad \text{Eq. 1}$$

where the blood cell activity concentration, C_{BC}, can be calculated from:

$$C_{BC}(t) = \frac{C_{WB}(t) - (1 - H)C_P(t)}{H}. \qquad \text{Eq. 2}$$

The value H represents hematocrit (assumed for each patient as $H = 0.39$). Before application of Equations 1 and 2, C_{BC} and C_P were expressed in Bq/kg of water, assuming that plasma contains 0.94 kg water/L and erythrocytes contain 0.73 kg/L (*19*).

Urine was collected as voided in the intervals between imaging (i.e., between 90–120 min and 140–260 min) and weighed for total excreted volume, and 3 aliquots (0.2 mL each) of each void were used to determine the total excreted activity of ^{18}F-TFB.

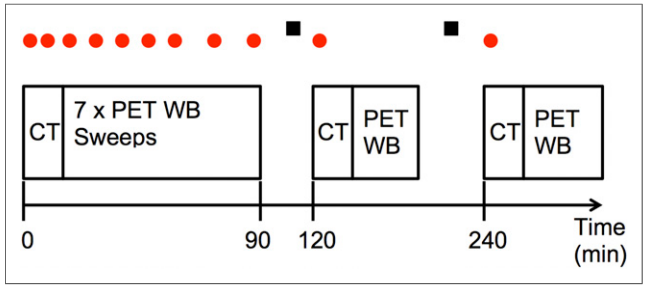

FIGURE 1. Imaging scan schedule for whole-body dynamic PET/CT study (not to scale). Dots above scan positions show timings of venous blood sampling, and squares represent nominal urine sampling times.

Image Reconstruction

Each whole-body PET image was attenuation-corrected using its corresponding CT image and included standard scanner-based corrections for decay, scatter, randoms, and dead-time. Each emission scan was reconstructed with a time-of-flight ordered-subset expectation maximization algorithm (2 iterations, 24 subsets), into a 256 × 256 matrix. A 4 mm in full width at half maximum gaussian postreconstruction smoothing filter was applied. The accuracy of the activity in the PET images was verified by summing the activity in the first whole-body PET scan and comparing with the decayed injected activity.

Absorbed Dose Calculations

Whole-body CT images from the 120- and 240-min PET/CT scans were rigidly registered to the 0- to 90-min CT using the PFUS package of PMOD (version 3.7; PMOD Technologies). The resulting transformations were then applied to the corresponding PET images. All PET frames were then merged to a single 4-dimensional series decay-corrected to a common time point. Organs of interest were identified and manually delineated by an experienced clinician using a fusion of both the corresponding CT and the PET images. A software correction was included to account for the imaging time of each bed position in the whole-body sweeps. Visible organs with high uptake or easily identified on CT images were the brain, thyroid, liver, spleen, stomach, heart, kidneys, lungs, testes (male only), and urinary bladder contents. Organ volumes were transferred to all frames, and independent volumes were adjusted where necessary to account for any movement of organs between different frames. All organs with the exception of the bladder were assumed to have a constant volume over time. The volume of the bladder was quantified on each PET scan using a 25% of maximum isocontour. PMOD software allows the automatic naming and standardized volume determination of each organ relating to the 70-kg Cristy–Eckerman adult anthropomorphic phantom used by the OLINDA/EXM dose calculation software, a software package widely used to obtain radiation dose estimates in radiopharmaceutical studies (*20*). Time–activity curves were produced for each organ, and using the PKIN package of PMOD (version 3.7). Organ normalized cumulated activities (NCA: numerically equivalent to the older terminology of residence time measured in MBq·h/MBq) were automatically calculated using the net injected activity and organ volume. Time–activity curves were fitted to biexponential functions where possible, assuming radionuclide decay (i.e., no further excretion) on reaching the last imaging point. Mean blood activity concentration was generated in calibrated kBq/mL from the average value of the 3 samples. Total blood activity was calculated assuming that 5.4% of the reference phantom's mass (70 kg) was blood. The blood time–activity curve was fitted with an exponential curve, the NCA determined, and this value used as the NCA for the red marrow in OLINDA calculations.

Summed activities of the urinary bladder and voided urine over the course of the study were fitted with a 1-phase exponential curve using the formula:

$$U(t) = U_{max} \times \left[1 - \exp\left(-\ln 2 \times \frac{t}{T_{1/2}}\right)\right], \qquad \text{Eq. 3}$$

where $U(t)$, U_{max}, and $T_{1/2}$ represent the accumulated urine activity at time t, maximum accumulated urine activity, and biologic half-life, respectively. From the fitting parameters, U_{max} and $T_{1/2}$ were determined and the NCA of the urinary bladder contents was calculated using a dynamic urinary bladder model in the OLINDA/EXM (version 1.1) software. A 3.5-h voiding interval was used as recommended by the International Commission on Radiological Protection (*21*). The remainder of body was assigned by activity not accounted for by organ delineation or excretion. Effective doses according to the tissue-weighting factors of International Commission on Radiological Protection publication 60 in each organ were calculated by inputting calculated NCAs into OLINDA/EXM. Absorbed doses to the 24 organs specified by the MIRD scheme in the target organs of the Cristy–Eckerman adult hermaphrodite male and female phantoms were determined, and sex-specific absorbed doses were averaged. Gonad-absorbed dose was taken to be the mean of the absorbed doses to the testes and ovaries. Absorbed doses to the salivary glands, which are not assigned organs in the OLINDA/EXM scheme, were also investigated. The submandibular and parotid glands were assigned a mass of 9.9 and 18 g, respectively, with a density of 1 g/cm^3 (values previously used for salivary gland dosimetric purposes (*22*)). NCAs for each gland from imaging were inputted into the Spheres module of the OLINDA/EXM software, and a curve of the form $d = a \times m^b$ was fitted to the resulting dose (mGy/MBq) to mass (g) relationship to determine the dose at the mass of the gland under investigation.

RESULTS

Safety

In all ^{18}F-TFB batches, radiochemical purity was greater than 99.8% as shown by radio-IC and radio-TLC, no silver was detected, radionuclidic purity was 100%, and no impurities were found. All batches were sterile and pyrogen free. The mean and SD of the administered mass of ^{19}F/^{18}F-TFB was 9 ± 4 μg, and the specific activity at the time of injection was 24 ± 13 MBq/μg. ^{18}F-TFB was found to be safe and well tolerated by all patients. There were no adverse or clinically detectable pharmacologic effects in any of the 5 subjects. No significant changes in vital signs or electrocardiograms were observed.

Biodistribution

Figure 2 shows the biodistribution of ^{18}F-TFB over time for a single representative patient. All patients showed similar biodistribution characteristics. The thyroid was clearly visible from the earliest time point, with uptake reaching a peak at approximately 30 min after injection for all patients. Outside the thyroid,

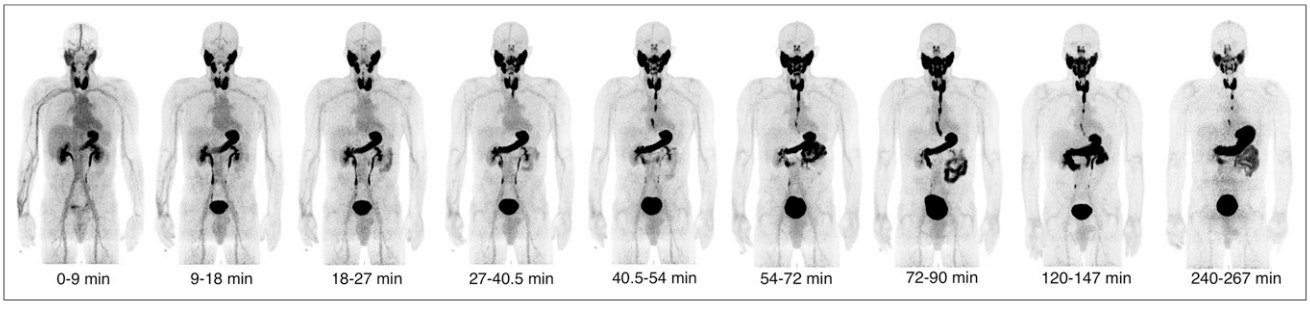

FIGURE 2. Decay-corrected serial maximum-intensity projections showing biodistribution of ^{18}F-TFB over course of imaging study. Thyroid, salivary gland, and stomach activities increase rapidly with time up to 30 min. Image captioned t = 0–9 min represents first imaging frame.

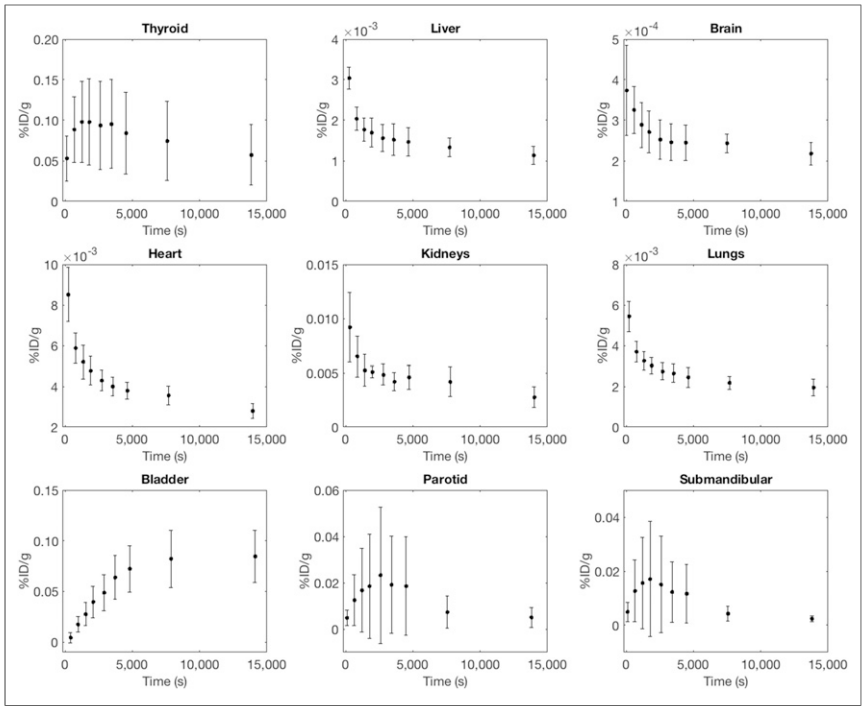

FIGURE 3. Percentage injected dose per gram of tissue (%ID/g) curves for selected organs, averaged over all 5 patients. Large SDs are evident in hNIS-expressing tissues and organs.

reconstructed images showed high uptake in other areas of elevated hNIS expression, such as the salivary glands and stomach. Excretion was primarily renal. Esophageal transit of ^{18}F-TFB was observed at later time points because saliva generated in the salivary glands is swallowed and enters the stomach and intestinal system. The oral cavity also showed increased activity 1 h after injection, probably due to pooling of saliva. Images showed low uptake in areas that do not significantly express hNIS, such as the brain and liver.

Tumor nodules ranging in size from 13 to 114 mm maximum diameter were photopenic against background healthy thyroid ^{18}F-TFB uptake, consistent with lower hNIS expression in differentiated thyroid cancer relative to normal thyroid. Persisting low-intensity blood-pool activity was observed on delayed images.

Figure 3 shows the average percentage injected activity over all patients for a range of organs considered for dosimetric purposes, and Figure 4 details the plasma and blood activity concentrations as well as the distribution ratio of the radiotracer.

Radiation Dosimetry

Using time–activity curves derived from biodistribution imaging, we first calculated mean NCA values (Supplemental Table 1; supplemental materials are available at http://jnm.snmjournals.org) and then determined the absorbed doses per unit administered activity to the MIRD scheme–listed organs, as established from OLINDA and averaged over all patients (Table 1). The highest absorbed organ doses were those to the thyroid, stomach, and bladder.

DISCUSSION

This work presents the first study, to our knowledge, of the biodistribution and radiation dosimetry of ^{18}F-TFB in humans. Previous work in primates (also using OLINDA and assuming distribution in the Cristy–Eckerman phantom) demonstrated a whole-body absorbed effective dose of 0.0247 ± 0.0028 mSv/MBq, which compares well with our calculated value of 0.0326 ± 0.0018 mSv/MBq averaged over men and women, despite physiologic differences between humans and primates. As evident in Figure 2, organs with the highest tracer uptake correspond to tissues associated with high hNIS expression. Increased uptake in the stomach reflects a combination of hNIS expression and swallowed saliva, after secretion by the salivary glands. Images are consistent with ^{18}F-TFB passing from the salivary glands into the mouth and through the esophagus into the stomach. The average mass of tetrafluoroborate injected (9 μg) corresponds to approximately 0.1 μmol, which assuming a total extracellular fluid volume (including plasma) of 15 L would lead to a maximum concentration of tetrafluoroborate in extracellular fluid of around 7 nM, much lower than the range of values reported for the 50% inhibitory concentration of tetrafluoroborate (~1 μM) (*10*). Therefore, it is unlikely that significant blocking of hNIS occurs in these studies despite reported concerns (*15*).

The large SD observed in the organs and tissues with high hNIS expression, such as the thyroid and salivary glands, shows that uptake in these tissues is variable among the small population studied. As detailed in Figure 4, blood and plasma sample counting shows that ^{18}F-TFB equilibrates between plasma and blood

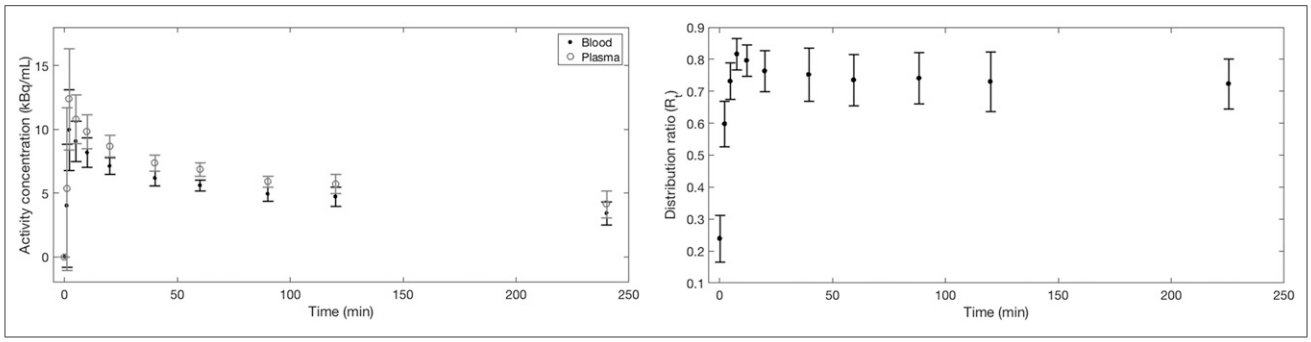

FIGURE 4. (Left) Mean decay-corrected blood and plasma curves averaged over all 5 patients. (Right) Mean blood cells to plasma distribution ratio, showing that equilibrium is reached after approximately 30 min. Error bars in both plots represent 1 SD of mean.

TABLE 1
Radiation Absorbed Doses for Organs Identified in MIRD Schema

Organ/tissue	Mean (mSv/MBq)	SD (mSv/MBq)
Gonads	0.020	0.014
Adrenals	0.015	0.003
Brain	0.005	0.001
Breasts	0.009	0.003
Gallbladder wall	0.015	0.004
Lower large intestine wall	0.016	0.004
Small intestine	0.014	0.003
Stomach wall	0.069	0.022
Upper large intestine wall	0.014	0.004
Heart wall	0.018	0.004
Kidneys	0.029	0.009
Liver	0.018	0.004
Lungs	0.011	0.003
Muscle	0.011	0.003
Pancreas	0.018	0.004
Marrow	0.034	0.003
Osteogenic cells	0.033	0.005
Skin	0.008	0.002
Spleen	0.020	0.003
Thymus	0.011	0.003
Thyroid	0.135	0.079
Urinary bladder wall	0.102	0.046
Uterus	0.019	0.004
Total body	0.011	0.003
*Parotid	0.031	0.011
*Submandibular	0.061	0.031
Effective dose	0.0326	0.0018

*Organs that are not in OLINDA model, with absorbed dose (in mGy/MBq) estimated from Spheres model within OLINDA/EXM software.

TABLE 2
Comparison of Whole-Body Effective Doses in mSv/MBq for Range of Radiotracers Used for Imaging of Thyroid

Radiopharmaceutical	Effective dose (mSv/MBq)	Nominal imaging activity (MBq) (*27*)
^{131}I-I$^-$	22*, 29†	3–10
^{123}I-I$^-$	0.23‡, 0.31¶	20
^{124}I-I$^-$	13‡, 18¶	50
^{99m}Tc-TcO$_4^-$	0.013§	80
^{18}F-TFB	0.0289	200
^{18}F-FDG	0.019	400

*Medium thyroid uptake, no blocking, oral administration, adult.
†High thyroid uptake, no blocking, oral administration, adult.
‡Medium thyroid uptake, no blocking, intravenous administration, adult.
¶High thyroid uptake no blocking, intravenous administration, adult.
§Intravenous administration, adult.
All values except ^{18}F-TFB are from ICRP publication 128 (*28*). ^{18}F-FDG value from (*29*).

cells, with the distribution ratio converging to a constant value of approximately 0.74 by 30 min.

Matched radionuclide pairs for diagnostic imaging and radionuclide treatment are an integral part of nuclear medicine and the field has attracted the name theranostics. ^{99m}Tc-TcO$_4^-$ is often used to estimate accumulation and trapping function before ^{131}I-I treatment of hyperthyroidism (*23*), the pattern and intensity of ^{99m}Tc-TcO$_4^-$ uptake indicating the etiology of hyperthyroidism (Grave's disease, multinodular goiter, thyroiditis). Comparisons have shown good imaging concordance between radioiodine and ^{99m}Tc-TcO$_4^-$ (*24,25*). Like ^{99m}Tc-TcO$_4^-$, ^{18}F-TFB is trapped but not organified by the thyroid. Further investigation of its potential as a diagnostic in hyperthyroidism and comparison with ^{99m}Tc-TcO$_4^-$ are warranted. ^{18}F-TFB may have applications for thyroid-stimulating hormone stimulated detection of differentiated thyroid cancer metastases after surgery and thyroid remnant ablation as an imaging partner for ^{131}I-I$^-$ therapy. By comparison with ^{124}I-I$^-$ PET, ^{18}F-TFB offers a low absorbed dose and favorable imaging characteristics that allow early imaging by comparison with ^{124}I-I$^-$ PET. ^{18}F-TFB may also have potential for the investigation of other hNIS-expressing tumor types such as breast and salivary gland cancers.

There are limitations with assuming organs and tissues as unit density spheres as used here for calculation of radiation doses to organs not present in the OLINDA models, with some reports showing differences in radiation dose of more than 100% between this method and gold standard Monte Carlo simulations (*26*). These differences mainly arise because of differences in tissue geometry compared with a true sphere. Although the unit density spheres model is only an approximation to clinical reality, our results are on the same order as previous works in primates, which also used the same methodology for calculation of the salivary gland doses (*17*) (literature values: parotid, 0.0413 mGy/MBq; submandibular gland, 0.0274 mGy/MBq).

In comparison to other commonly used radiotracers used in thyroid imaging, Table 2 shows that ^{18}F-TFB delivers a much lower absorbed radiation dose than the radioiodine family of tracers for both medium and high levels of thyroid uptake. Image quality within 1 h of administration (mean administered activity, 185 MBq) was consistently excellent in this pilot study. Future studies may be able to optimize the injected activity.

CONCLUSION

^{18}F-TFB is an hNIS substrate analogous in biodistribution to ^{99m}Tc-pertechnetate and is taken up selectively in hNIS-expressing tissues. It is safe to administer in humans, and its biodistribution and dosimetry warrant further clinical evaluation as a PET tracer for imaging thyroid pathophysiology and hNIS expression.

DISCLOSURE

This study was funded by an MRC Confidence in Concept grant administered by King's Health Partners. Financial support was

also received from the Department of Health via the National Institute for Health Research (NIHR) comprehensive Biomedical Research Centre award to Guy's & St Thomas' NHS Foundation Trust in partnership with King's College London and King's College Hospital NHS Foundation Trust under grant number WT088641/Z/09/Z. This study was also supported by the Centre of Excellence in Medical Engineering Centre funded by the Wellcome Trust and EPSRC under grant number WT088641/Z/09/Z, and the King's College London and UCL Comprehensive Cancer Imaging Centre funded by CRUK and EPSRC in association with the MRC and DoH (England) (C1519/A16463). The views expressed are those of the authors and not necessarily those of the NHS, the NIHR, the DoH, EPSRC, or Wellcome Trust. No other potential conflict of interest relevant to this article was reported.

ACKNOWLEDGMENTS

We thank the radiography staff at the PET Centre at St Thomas' Hospital for their help in collecting the data and radiochemistry staff for radiotracer production.

REFERENCES

1. Chung J-K. Sodium iodide symporter: its role in nuclear medicine. *J Nucl Med.* 2002;43:1188–1200.
2. Silberstein EB, Alavi A, Balon HR, et al. The SNMMI practice guideline for therapy of thyroid disease with ^{131}I 3.0. *J Nucl Med.* 2012;53:1633–1651.
3. Phan HT, Jager PL, Paans AM, et al. The diagnostic value of ^{124}I-PET in patients with differentiated thyroid cancer. *Eur J Nucl Med Mol Imaging.* 2008;35:958–965.
4. Gulec SA, Kuker RA, Goryawala M, et al. ^{124}I PET/CT in patients with differentiated thyroid cancer: clinical and quantitative image analysis. *Thyroid.* 2016; 26:441–448.
5. Woods DH, Woods SA, Woods MJ, et al. The standardization and measurement of decay scheme data of ^{124}I. *Appl Radiat Isot.* 1992;43:551–560.
6. Schmitz J. The production of [^{124}I]iodine and [^{86}Y]yttrium. *Eur J Nucl Med Mol Imaging.* 2011;38(suppl 1):S4–S9.
7. Johansson L, Mattsson S, Nosslin B, Leide-Svegborn S. Effective dose from radiopharmaceuticals. *Eur J Nucl Med.* 1992;19:933–938.
8. Anbar M, Guttman S, Lewitus Z. Effect of monofluorosulphonate, difluorophosphate and fluoroborate ions on the iodine uptake of the thyroid gland. *Nature.* 1959;183:1517–1518.
9. Waltz F, Pillette L, Ambroise Y. A nonradioactive iodide uptake assay for sodium iodide symporter function. *Anal Biochem.* 2010;396:91–95.
10. Khoshnevisan A, Chuamsaamarkkee K, Boudjemeline M, et al. ^{18}F-fluorosulfate for PET imaging of the sodium/iodide symporter: synthesis and biological evaluation in vitro and in vivo. *J Nucl Med.* 2017;58:156–161.
11. Anbar M, Inbar M. *The Application of F18 Labelled Fluoroborate Ions to Problems in Thyroid Physiology.* Tel-Aviv, Israel: Israel Atomic Energy Commission; 1962.
12. Askenasy HM, Anbar M, Laor Y, Lewitus Z, Kosary IZ, Guttmann S. The localization of intracranial space-occupying lesions by fluoroborate ions labelled with fluorine 18. *AJR.* 1962;88:350–354.
13. Entzian W, Aronow S, Soloway AH, Sweet WH. A preliminary evaluation of F-18-labelled tetrafluoroborate as a scanning agent for intracranial tumors. *J Nucl Med.* 1964;5:542–550.
14. Jauregui-Osoro M, Sunassee K, Weeks AJ, et al. Synthesis and biological evaluation of [^{18}F]tetrafluoroborate: a PET imaging agent for thyroid disease and reporter gene imaging of the sodium/iodide symporter. *Eur J Nucl Med Mol Imaging.* 2010;37:2108–2116.
15. Khoshnevisan A, Jauregui-Osoro M, Shaw K, et al. [^{18}F]tetrafluoroborate as a PET tracer for the sodium/iodide symporter: the importance of specific activity. *EJNMMI Res.* 2016;6:1–10.
16. Weeks AJ, Jauregui-Osoro M, Cleij M, Blower JE, Ballinger JR, Blower PJ. Evaluation of [^{18}F]-tetrafluoroborate as a potential PET imaging agent for the human sodium/iodide symporter in a new colon carcinoma cell line, HCT116, expressing hNIS. *Nucl Med Commun.* 2011;32:98–105.
17. Martí-Climent JM, Collantes M, Jauregui-Osoro M, et al. Radiation dosimetry and biodistribution in non-human primates of the sodium/iodide PET ligand [^{18}F]-tetrafluoroborate. *EJNMMI Res.* 2015;5:70.
18. Nahmias C, Wahl LM, Amano S, Asselin M-C, Chirakal R. Equilibration of 6-[^{18}F]fluoro-L-m-tyrosine between plasma and erythrocytes. *J Nucl Med.* 2000; 41:1636–1641.
19. Siggaard-Andersen O. *The Acid-Base Status of the Blood.* 4th ed. Copenhagen, Denmark: Munksgaard; 1976.
20. Stabin MG, Sparks RB, Crowe E. OLINDA/EXM: the second generation personal computer software for internal dose assessment in Nuclear Medicine. *J Nucl Med.* 2005;46:1023–1027.
21. International Commission on Radiological Protection. Age-dependent doses to members of the public from intake of radionuclides: part 1. ICRP publication 56. *Ann ICRP.* 1992;20:2.
22. Jentzen W, Hobbs RF, Stahl A, Knust J, Sgouros G, Bockisch A. Pre-therapeutic ^{124}I PET(/CT) dosimetry confirms low average absorbed doses per administered ^{131}I activity to the salivary glands in radioiodine therapy of differentiated thyroid cancer. *Eur J Nucl Med Mol Imaging.* 2010;37:884–895.
23. Sucupira MS, Camargo EE, Nickoloff EL, Alderson PO, Wagner HNJ. The role of ^{99m}Tc pertechnetate uptake in the evaluation of thyroid function. *Int J Nucl Med Biol.* 1983;10:29–33.
24. Reschini E, Catania A, Ferrari C, Bergonzi M, Paracchi A, Raineri P. Comparison of pertechnetate and radioiodine thyroid scintiscans in thyroid disease. *J Nucl Biol Med.* 1993;37:12–17.
25. Krishnamurthi GT, Shoop L, Walsh C, Blahd WH. Comparison of 99mtechnetium pertechnetate and radioiodine (I-131) as thyroid scanning agents. *Nuklearmedizin.* 1973;1973:97–106.
26. O'Doherty J, Clauss R, Scuffham J, Khan A, Petitguillaume A, Desbree A. Three dosimetry models of lipoma arborescens treated by ^{90}Y synovectomy. *Med Phys.* 2014;41:052501.
27. Administration of Radioactive Substances Advisory Committee. Notes for guidance on the clinical administration of radiopharmaceuticals and use of sealed radioactive sources. In: Department of Health, ed. *ARSAC Notes for Guidance: Good Clinical Practice in Nuclear Medicine*. London, U.K.: Administration of Radioactive Substances Advisory Committee; 2016.
28. Mattsson S, Johansson L, Leide-Svegborn S, et al. Radiation dose to patients from radiopharmaceuticals: a compendium of current information related to frequently used substances. ICRP publication 128. *Ann ICRP.* 2015;44(2S).
29. Delbeke D, Coleman RE, Guiberteau MJ, et al. Procedure guideline for tumor imaging with ^{18}F-FDG PET/CT 1.0*. *J Nucl Med.* 2006;47:885–895.